Inorganic Chemistry

Article

pubs.acs.org/IC

Graphene/Acid Coassisted Synthesis of Ultrathin MoS_2 Nanosheets with Outstanding Rate Capability for a Lithium Battery Anode

Kan Zhang,[†] Hwan-Jin Kim,[‡] Xinjian Shi,[‡] Jeong-Taik Lee,[†] Jae-Man Choi,[§] Min-Sang Song,*[,§] and Jong Hyeok Park*[,†,‡]

[†]SKKU Advanced Institute of Nanotechnology (SAINT), Sungkyunkwan University, Suwon 440-746, Republic of Korea

[‡]School of Chemical Engineering, Sungkyunkwan University, Suwon 440-746, Republic of Korea

[§]Energy Storage Group, Materials R&D Center, Samsung Advanced Institute of Technology, Yongin 446-712, Republic of Korea

Supporting Information

ABSTRACT: Morphology-controlled MoS_2 nanosheets were successfully synthesized with the aid of graphene/acid coexistence by a one-pot hydrothermal method. The ultrathin MoS_2 nanosheets were self-assembled into a cockscomb-like structure with an exposed (100) facet on graphene sheets, which is in strong contrast to large aggregate MoS_2 plates grown freely on graphene sheets without acetic acid. The ultrathin MoS_2 nanosheets displayed excellent rate performance for Li storage (709 $mAh{\cdot}g^{-1}$ capacity at 8320 $mA{\cdot}g^{-1}$ discharging rate) and superior charge/discharge cyclability.

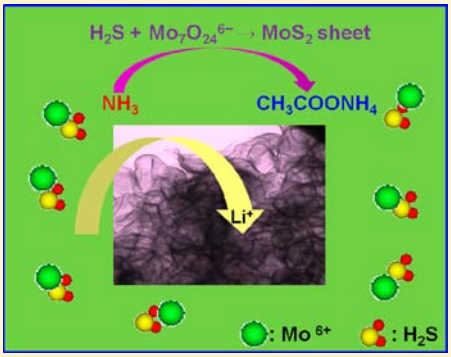

INTRODUCTION

The unique properties and various applications of two-dimensional (2-D) layered nanomaterials have resulted in increasing attention for scientific and technological interests.[1−5] Among them, graphene-like transition metal sulfides (TMS), such as MoS_2, WS_2, ZrS_2, and SnS_2, are of particular interest as alternatives for graphite anode materials used in commercial lithium ion batteries (LIBs) due to their high theoretical capacities and safer operation.[6−9] The high practical capacities and fast Li ion movement in TMS originate from two main reasons with respect to the mechanism of Li ion storage. The weak van der Waals bounded layer structure (S-metal-S) can induce easy intercalation/deintercalation of Li ions, lowering the energy barrier for Li ion movement,[10,11] and the transition metal compound can store a large number of Li ions through a conversion reaction.[12,13] However, the poor cyclic stability hinders their use as the alternative anode material for LIBs. For example, the specific capacity of WS_2 sheets decayed to 63% of its initial value after 30 cycles,[14] and the specific capacity of the exfoliated MoS_2 sheets decreased to 70% of its initial value after 50 cycles.[15] The poor long-term cycle stability of TMS was due to the large volume change during the charge/discharge process, which causes pulverization of electrodes and thus deteriorates anode performance.[16,17] Moreover, the graphene-assisted MoS_2 compounds only yielded a 250 $mAh{\cdot}g^{-1}$ specific capacity at a 10 000 $mA{\cdot}g^{-1}$ discharging rate, which is also an insufficient rate capability for commercialization.[18]

The current strategies for solving these undesired issues of TMS involve controlling their nanostructures[7−9,19−21] or constructing controlled open channels.[15,21−24] Nanohybridized graphene sheets with TMS seem to be an effective approach because graphene with a high surface area can influence the morphology of TMS during synthesis. Moreover, the high electronic conductivity of graphene can promote intercalation of Li ions, and a nanoscale 2-D layered structure provides a large surface area that enhances Li ion transfer.[25−31] In this study, graphene/acid coassisted, one-pot synthesis of morphology-controlled ultrathin MoS_2 nanosheets is reported. With the synergistic effects from graphene and acetic acid, MoS_2-based composite nanomaterials exhibited an exceptionally high performance rate and excellent cyclability for Li ion storage.

EXPERIMENTAL SECTION

Materials. Graphite powder (purity 99.9999%) was obtained from Alpha Aesar. Other chemical reagents were purchased from Aldrich without further purification.

Synthesis of Graphene Oxide. GO was prepared using Hummer's method.[32] Briefly, graphite powder (1 g) was dispersed in cold, concentrated sulphuric acid (25 mL, 98 wt %, ice bath) containing 1 g of $NaNO_3$, and potassium permanganate ($KMnO_4$, 3 g) was slowly added with continuous vigorous stirring and cooling to prevent the temperature from exceeding 20 °C. The ice bath was removed and replaced by a water bath, and the mixture was heated to 35 °C for 1 h to release gas under continuous stirring, followed by the slow addition of deionized water (50 mL) that produced a rapid increase in the solution temperature to a maximum of 98 °C. The reaction was maintained for 12 h to increase the oxidation degree of

Received: March 25, 2013
Published: August 13, 2013

   dx.doi.org/10.1021/ic400735f | Inorg. Chem. 2013, 52, 9807−9812

the GO product. The resultant bright-yellow suspension was terminated by the addition of distilled water (140 mL), followed by a hydrogen peroxide solution (H_2O_2, 30%, 3 mL). The solid product was separated by centrifugation and washed with 200 mL of a 1:10 HCl solution, and water until pH = 7. The powder was then vacuum-dried at room temperature.

Synthesis of Ultrathin MoS_2/Graphene Composites. The synthesis of ultrathin MoS_2/graphene composites was based on a chemical modification procedure previously reported.[21] First, GO was dispersed in 35 mL of water by ultrasonication for 1 h. Afterward, 0.23 g of $(NH_4)_6Mo_7O_{24}$ and 0.3 g of thiourea were added with vigorous stirring for 2 h. The pH of the reaction system was neutralized by adding 1 M NaOH. To suppress growth of MoS_2 sheets along the *c*-axis, 1 mL of glacial acetic acid was added to maintain the pH, and then the sample was transferred to a 50 mL Teflon autoclave, sealed, and maintained at 240 °C for 12 h. During this hydrothermal reaction, the GO can be completely reduced to graphene in the presence of NaOH as a reducing agent.[33] The resulting composite was washed with water and acetone two times and then dried at 50 °C. For comparison, the pure MoS_2 sheets were synthesized without graphene. General MoS_2 nanoplates with and without graphene were synthesized without adding glacial acetic acid.

Analysis Instruments. Scanning electron microscopy (SEM) images of the product were taken with a field emission scanning electron microscope (FE-SEM, JSM-7000F, Japan). X-ray diffraction (XRD) patterns were obtained with a diffractometer D500/5000 in Bragg-Bretano geometry under Cu Kα radiation. X-ray photoelectron spectroscopy (XPS) was conducted on an AESXPS instrument (ESCA2000, VG Microtech, England) equipped with an aluminum anode (Al Kα = 1486.6° eV). Transmission electron microscopy (TEM) and high-resolution transmission electron microscopy (HRTEM) observations were performed on a JEOL JEM-2100F (Japan) electron microscope. Raman spectra were acquired at room temperature using an excitation energy of 2.41 eV (514 nm, Ar+ ion laser, Renishaw, RM-1000 Invia). Brunauer–Emmett–Teller (BET) specific surface areas and porosity of the samples were evaluated on the basis of nitrogen adsorption isotherms measured at −196 °C using a gas adsorption apparatus (ASAP 2020, Micromeritics, Norcross, GA). Thermogravimetric analysis (TGA) was conducted using a Seiko Exstar 6000 in air atmosphere and heated at a rate of 10 °C/min.

Preparation of Electrodes. Composite electrodes were prepared by mixing a powder sample, carbon black (Super P), and poly(vinylidene fluoride) (PVdF) dissolved in *N*-methyl-2-pyrrolidone (NMP) at a 85:10:5 weight ratio. Carbon black was used as a conductive additive, and PVdF was added as a binder. The mixed active material was deposited on copper foil as a current collector, followed by vacuum drying at 120 °C for 12 h. The cell electrolyte was $LiPF_6$ (1 M) with ethylene carbonate (EC)/diethylene carbonate (DEC)/ethyl-methyl carbonate (EMC) (1:1:1 (v/v/v), Techno SEMICHEM Co., Ltd., Korea). All cells were constructed and handled in an Ar-filled glovebox. Electrochemical properties were analyzed with two electrode cells using an electrochemical analyzer (CHI 660), and Li metal was used as counter electrode and reference electrode.

RESULTS AND DISCUSSION

Two-dimensional MoS_2 nanoplates (hereafter, NP) can be synthesized with a high yield by a simple hydrothermal strategy in the presence of graphene oxide (GO) as previously reported.[22,24,34] To hybridize MoS_2 NP with graphene nanosheets, the hydrothermal reaction was controlled to occur along with the GO reduction. Multilayered MoS_2 NPs have a strong tendency to aggregate due to high van der Waals stacking of the MoS_2 NP in the (002) plane as shown in Figure S1a, Supporting Information. However, synthesized MoS_2 NP/graphene without the assistance of acetic acid displays a 3-D architecture morphology with enhanced porosity (Figure S1b–d). FE-SEM images of the composite MoS_2 synthesized by coassistance of graphene and acetic acid are shown in Figure 1a,b. For comparison, FE-SEM images of MoS_2 synthesized

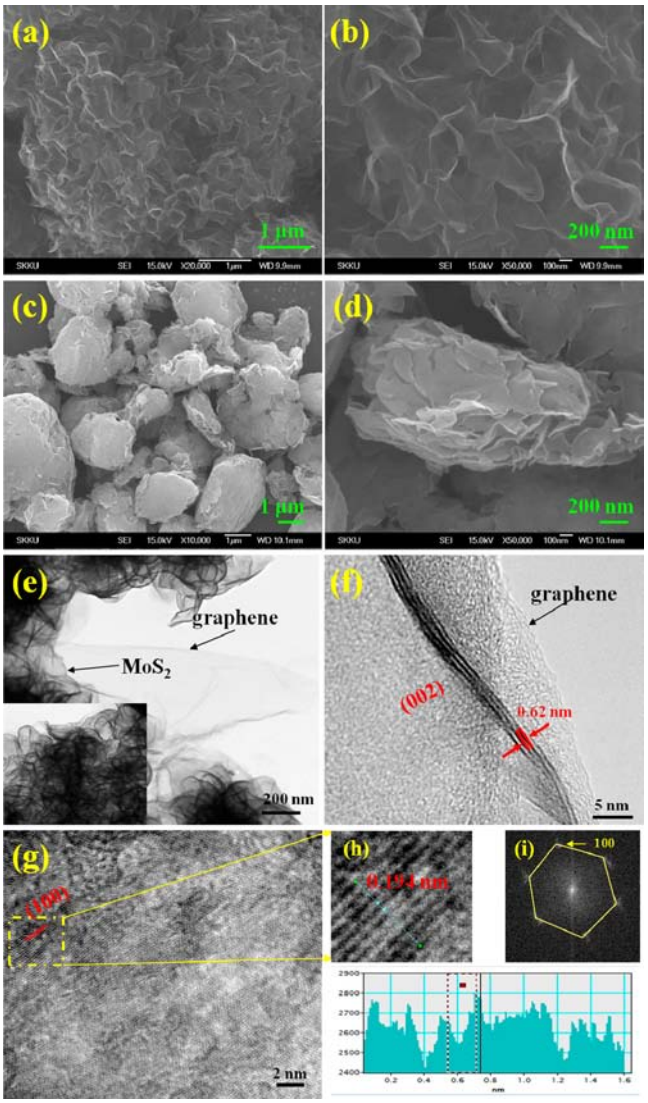

Figure 1. SEM images of MoS_2 NS with (a, b) 3 wt % graphene and (c, d) without graphene. (e) TEM and (f–h) HR-TEM images and selected area electron diffraction (SAED) (i) pattern of 3 wt % MoS_2 NS/graphene.

with acetic acid are also shown in Figure 1c,d. The coassisted MoS_2 nanosheets (hereafter, NS) have much improved porosity compared to other samples. Although the acetate treatment process is followed in recent reports on the preparation of 2-D nanosheet materials,[35−37] the formation mechanism of these 2-D materials by the assistance of acetic acid is currently unclear. It was previously demonstrated that some additive organic agents, including acetic acid, can influence the stability, morphology, and growth habits of crystals.[35] In this study, acetic acid could play a buffering role during the MoS_2 formation reaction to maintain the pH. Raw materials, $(NH_4)_6Mo_7O_{24}$ and thiourea, could release ammonia at an elevated temperature during the hydrothermal synthesis, which leads to an increase in the reaction environment pH.[38] The addition of acetic acid is expected to react with ammonia and form ammonium acetate to maintain the initial pH value. Interestingly, individual ultrathin MoS_2 nanosheets with 3 wt %

dx.doi.org/10.1021/ic400735f | Inorg. Chem. 2013, 52, 9807−9812

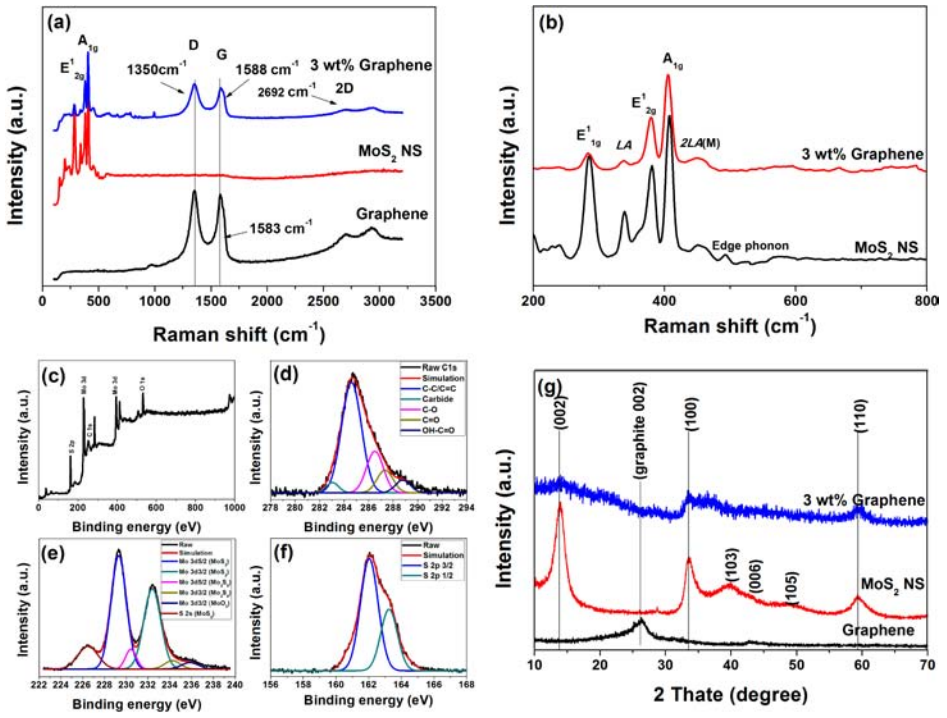

Figure 2. Raman spectra of (a, b) graphene, MoS_2 NS, and 3 wt % MoS_2 NS/graphene, and (c) full XPS spectrum of 3 wt % MoS_2 NS/graphene. (d) C1s deconvolution spectra, (e) Mo 3d deconvolution spectra, (f) S 2p deconvolution spectra, and (g) XRD patterns of graphene, MoS_2 NS and 3 wt % MoS_2 NS/graphene.

graphene (this mass fraction was obtained from stoichiometric ratio between Mo precursor and graphene) looks like a cockscomb with a smooth surface and no obvious aggregation as shown in Figure 1a,b, indicating that the graphene sheets act as dispersing agents to promote the formation of porous composites and reduce aggregation.

The TEM image of MoS_2 NS/graphene shows that MoS_2 NS was well dispersed in the composite materials (Figure 1e). A typical HRTEM image of the planar sheet results in a prediction of 3−4 layers and a 0.62 nm interlayer spacing of MoS_2 NS in the presence of graphene sheets, respectively. The HR-TEM image of pure MoS_2 NS (without graphene) indicates more layers (~8 layers) than the MoS_2 NS/graphene composite as shown in Figure S2, Supporting Information. In addition, the HR-TEM image of the (100) plane of a typical MoS_2 NS in the MoS_2 NS/graphene has a 0.194 nm lattice spacing (Figure 2g,h), and the electron diffraction pattern of a flat area of the nanosheet (Figure 2i) shows a hexagonal lattice structure,[20] confirming a well-developed MoS_2 structure.

The natural exfoliated GO showed microsized sheets with high oxygen-containing functional groups that were confirmed by AFM, TEM, XRD, XPS, and Raman studies (Figure S3a−f, Supporting Information). The Raman spectrum of graphene derived from the reduction of GO shows two prominent bands at 1583 cm^{-1} (G band) and 1350 cm^{-1} (D band), which corresponds to the vibration of sp^2-bonded carbon atoms and the dispersive, defect-induced vibrations, respectively (Figure 2a). The G band of graphene up-shifted to 1588 for 3 wt % MoS_2 NS/graphene, which may be evidence of chemical doping of carbon materials and further corroborates previous studies of p-type doping of graphene causing an upshift of the G band.[39] In addition, the G band upshift provides reliable evidence that there will be electronic interaction between graphene and MoS_2 sheets in the composite, resulting in a dyadic bonding between graphene and MoS_2.[40,41] The Raman spectra of the MoS_2 NS and MoS_2 NS/graphene composite illustrate the characteristic peaks at 373 ($E^1_{2g}(\Gamma)$) and 400 cm^{-1}($A_{1g}(\Gamma)$), respectively.[42] The uniform formation of MoS_2 on graphene was further confirmed by the resonance Raman spectra of MoS_2, as shown in Figure 2b. The appearance of E1 1g, E1 2g, LA, 2LA(M), and A1g are associated with the vibration of one MoS_2 layer against neighboring layers and is called the rigid layer mode.[43] The full-scale XPS spectrum of the MoS_2 NS/graphene composite shows C1s at ~286.4 eV, O1s at ~532.2 eV, Mo3d at ~232.1 eV, and S2p at ~162.8 eV (Figure 2c). As shown in Figure 2d, the high-resolution XPS spectrum of the C1s region indicates considerable deoxygenation compared to GO (Figure S3f, Supporting Information). In addition, the peak with the binding energy of 283 eV can be assigned to the carbide bond for the MoS_2 NS/graphene composite, indicating a chemical interaction between graphene and MoS_2, which is consistent with the Raman characterization of the G band upshift. The deconvoluted Mo 3d and S 2p spectra clearly indicate the formation of crystalline MoS_2, and the low intensity of Mo 3d signals, presumably due to Mo_2S_5, is attributed to an intermediate product in the MoS_3-to-MoS_2 transition (Figure 2e,f).[44] XRD patterns of graphene, MoS_2 NS, and MoS_2 NS/graphene are compared in Figure 2g. Generally, the (002) reflection in lamellar structured materials can be ascribed to layers stacked along the (002) direction. Therefore, the (002) plane peak can be detected in both pure graphene and MoS_2 NS, indicating that they have many layers ordered along the (002) stacking direction. The (002) plane peak nearly disappeared in MoS_2 NS/graphene, suggesting that the number of (002) planes in MoS_2 decreased after graphene introduction, which resulted in ultrathin MoS_2 nanosheets, such as the graphene structure.[45,6] The formation process of the MoS_2 NS/graphene composite is schematically illustrated in Figure S4.

dx.doi.org/10.1021/ic400735f | Inorg. Chem. 2013, 52, 9807−9812

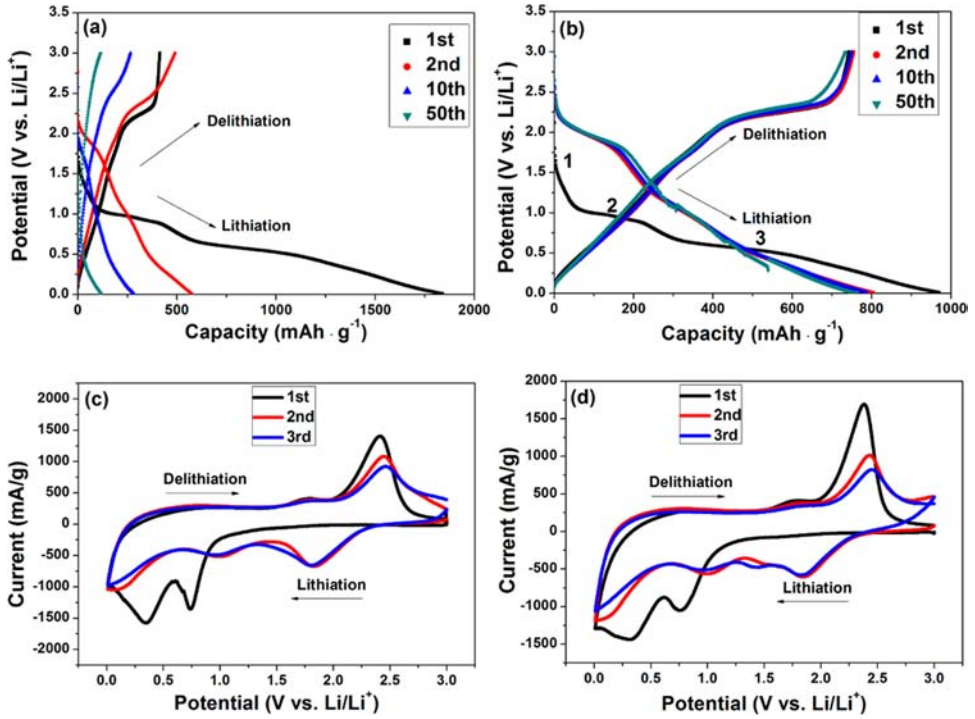

Figure 3. Voltage profiles for (a) MoS_2 NS and (b) 3 wt % MoS_2 NS/graphene cycled at a rate of 0.5 C between 3 and 0 V vs Li/Li^+. Cyclic voltammograms of (c) MoS_2 NS and (d) 3 wt % MoS_2 NS/graphene at a scanning rate of 0.5 mV/s during the first three cycles.

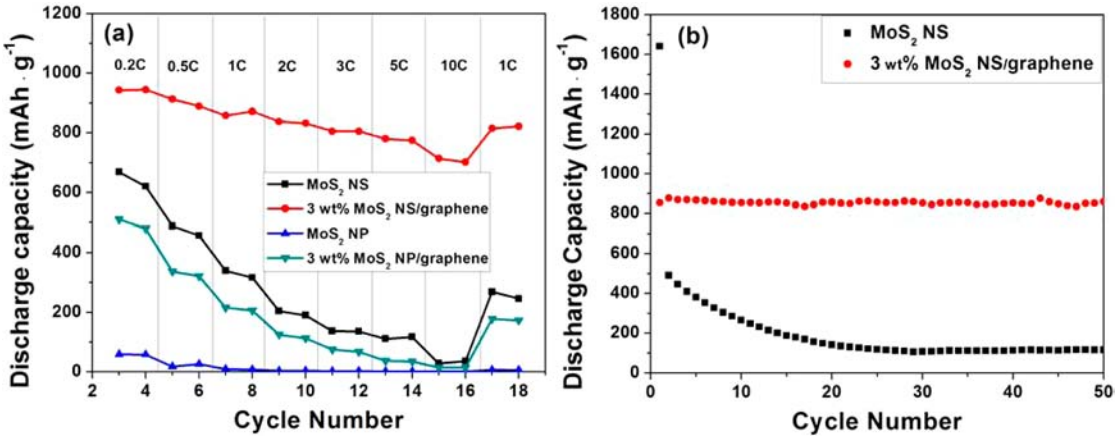

Figure 4. Cycling performance of different kinds of MoS_2 and 3 wt % MoS_2/graphene at (a) various current densities and the variation in discharge capacity vs cycle number for (b) MoS_2 NS and 3 wt % MoS_2 NS/graphene.

The charge/discharge characteristics were tested by galvanostatically cycling the cells based on the current density calculated by 1 C (1C = ~832 $mA{\cdot}g^{-1}$) in the potential range of 0−3 V vs Li/Li^+, and the whole capacity is calculated based on the total weight of the composite (approximate 4.8% graphene content in composite by TGA analysis in Figure S5). The MoS_2 NS and 3 wt % MoS_2 NS/graphene composite behaviors are shown in Figure 3a,b. For 3 wt % MoS_2 NS/graphene at the first cycle, the charge (lithiation) and discharge (delithiation) capacities are 970.4 and 742.9 $mAh{\cdot}g^{-1}$, while that of MoS_2 NS are 1838.9 and 413.3 $mAh{\cdot}g^{-1}$. As a result, the coloumbic efficiency of 3 wt % MoS_2 NS/graphene and MoS_2 NS were 76.5 and 22.5%, respectively. The cyclic voltammetry (CV) curves of MoS_2 NS and 3 wt % MoS_2 NS/graphene composites are shown in Figure 3c,d. The dominant reduction potential at approximately 0.31 and 0.75 V for MoS_2 NS/graphene could be attributed to a change in the coordination of Mo by six S atoms from a trigonal prismatic to an octahedral by inserting Li ions into the MoS_2 layers, and converting the reaction process of $MoS_2 + 4Li \rightarrow Mo + 2Li_2S$ during the first cycle.[18,46,47] After the first cycle, pristine MoS_2 was converted to a mixture of S and Mo, and thus two new peaks at 1.9 and ~1.1 V corresponding to the formation of Li_2S and the association of Li without Mo appeared.[18] This CV behavior is consistent with that of MoS_2 NS, indicating the same electrochemical reaction pathway with MoS_2 NS despite the ultrathin MoS_2 NS with only 3−4 layers.[18]

Excellent C-rate performance is crucial to achieving high power densities in LIBs. High reversible capacities of MoS_2 NS/graphene were exhibited with the variation of current density, as shown in Figure 4a. For example, 3 wt % MoS_2 NS/graphene shows discharge capacities (delithiation) of approx-

dx.doi.org/10.1021/ic400735f | Inorg. Chem. 2013, 52, 9807−9812

imately 946, 889, 875, 835, 808, 774, and 709 mAh·g^{-1} at various C-rates of 0.2, 0.5, 1, 2, 3, 5, and 10 C, respectively. The capacity remains at 709 mAh·g^{-1} for a 10 C (8320 mA·g^{-1}) discharge rate, meaning only 25% decay occurs when the current density is increased 20-fold. MoS_2 NS prepared using only acetic acid as an additive and MoS_2 NP/graphene prepared using only graphene as an additive exhibited very poor performance rates, which illustrate the synergistic effects of the coassisted synthesis. The excellent performance rate for Li storage is the highest reported for graphene-based composites. For example, NiO sheets grown on graphene were 492 mAh·g^{-1} for a 3590 mA·g^{-1} rate,[48] Co_3O_4/graphene with a sheet-on-sheet structure has a ~410 mAh·g^{-1} capacity at a 4450 mA·g^{-1} rate,[49] and MoS_2/PEO/graphene exhibited a rate capability with rates as high as 10 000 mA·g^{-1} yielding ~250 mA·g^{-1}.[18] Moreover, the rate does not reduce the specific capacity when the current density changes back to 1 C, indicating excellent cyclability. However, the discharge capacities of MoS_2 NP, NS, and MoS_2 NP/graphene show a nearly 100% decrease when the discharge C-rate increases from 0.2 to 10 C. Furthermore, to understand the real role of graphene in the composite, the rate capability of the MoS_2 NS and 3 wt % MoS_2 NS/graphene electrodes fabricated without carbon black was shown in Figure S6, Supporting Information. Therefore, the extremely high rate performance of MoS_2 NS/graphene composites is primarily due to synergistic effects based on the porous nature of the ultrathin MoS_2: (1) a high effective interaction area between MoS_2 and the electrolyte due to a high surface to volume ratio and great porosity. The porous morphology of the composites were confirmed by nitrogen isothermal adsorption (Figure S7, Supporting Information); (2) a narrowed Li diffusion path; (3) increasing contact area for electron transfer between MoS_2 and graphene due to the ultrathin sheets; and (4) enhanced kinetics of the charge carrier transport due to the high conductivity of graphene.

The cycling performance of MoS_2 NS/graphene was also plotted in Figure 4b. At a discharge current density of 1 C, the specific capacity of MoS_2 NS shows a rapid decrease during the initial 30th cycle. However, the specific capacity of 3 wt % MoS_2 NS/graphene could be maintained at 860 mA·g^{-1} during the 50th cycle, suggesting that graphene and the ultrathin morphology significantly improved the specific capacities and cyclic stabilities of the MoS_2 NS. To understand the excellent cycle performance of the 3 wt % MoS_2 NS/graphene composite, the morphology variation of the MoS_2 NS and MoS_2 NS/graphene composites after 50 discharge/charge cycles was compared with SEM (Figure S8, Supporting Information). The ultrathin MoS_2 NS in the composite did not exhibit agglomeration or a morphology variation, indicating the introduction of graphene can effectively buffer the strain and stress of the volume change and prevent the detachment and agglomeration of pulverized MoS_2 NS during cycling, thereby enhancing the cyclic stability and rate capability.

CONCLUSIONS

In summary, MoS_2 nanosheets with controlled morphology via graphene/acid coexistence were successfully synthesized by a one-pot hydrothermal method. The synergistic effects of the use of graphene sheets and acetic acid during the one-pot hydrothermal reaction produced a highly porous, cockscomb-like nanostructure, and the resulting ultrathin MoS_2 NS/graphene composites displayed excellent performance rates and charge/discharge cyclability. These results significantly contribute to the commercial utilization of MoS_2 as an anode material for LIBs.

ASSOCIATED CONTENT

Supporting Information

FE-SEM images of MoS_2 NP and 3% MoS_2 NP/graphene, TEM images of MoS_2 NS, AFM, TEM, FT-IR, Raman and XPS of GO, TGA analysis of MoS_2 NS and 3 wt % MoS_2/graphene composite, the rate capabilities for MoS_2 NS, and 3 wt % MoS_2/graphene electrode without carbon black, Nyquist plots of the MoS_2 NS and MoS_2 NS/graphene, Nitrogen adsorption-desorption isotherms of MoS_2 NS and MoS_2 NS/graphene composite, FE-SEM images of MoS_2 NS and 3% MoS_2 NS/graphene after 50 time cycle. This material is available free of charge via the Internet at http://pubs.acs.org.

AUTHOR INFORMATION

Corresponding Author

*E-mail: lutts@skku.edu (J.H.P.), minsang77.song@samsung.com (M.S.S.).

Notes

The authors declare no competing financial interest.

ACKNOWLEDGMENTS

This work was supported by the NRF of Korea Grant funded by the Ministry of Science, ICT & Future Planning (NRF-2009-C1AAA001-2009-0094157, NRF-2013R1A2A1A09014038).

REFERENCES

(1) Armstrong, A. R.; Bruce, P. G. *Nature* **1996**, *381*, 499.
(2) Takada, K.; Sakurai, H.; Takayama-Muromachi, E.; Izumi, F.; Dilanian, R. A.; Sasaki, T. *Nature* **2003**, *422*, 53.
(3) Liu, Z. P.; Ma, R. Z.; Osada, M.; Iyi, N.; Ebina, Y.; Takada, K.; Sasaki, T. *J. Am. Chem. Soc.* **2006**, *128*, 4872.
(4) Chen, C. H.; Crisostomo, V. M. B.; Li, W. N.; Xu, L. P.; Suib, S. L. *J. Am. Chem. Soc.* **2008**, *130*, 14390.
(5) Zeng, Z. Y.; Yin, Z. Y.; Huang, X.; Li, H.; He, Q. Y.; Lu, G.; Boey, F.; Zhang, H. *Angew. Chem., Int. Ed.* **2011**, *50*, 11093.
(6) Ramakrishna Matte, H. S. S.; Gomathi, A.; Manna, A. K.; Late, D. J.; Datta, R.; Pati, S. K.; Rao, C. N. R. *Angew. Chem., Int. Ed.* **2010**, *49*, 4059.
(7) Seo, J.; Jang, J.; Park, S.; Kim, C.; Park, B.; Cheon, J. *Adv. Mater.* **2008**, *20*, 4269.
(8) Hwang, H. S.; Kim, H. J.; Cho, J. *Nano Lett.* **2011**, *11*, 4826.
(9) Jang, J. T.; Jeong, S. H.; Seo, J. W.; Kim, M. C.; Sim, E. J.; Oh, Y. H.; Nam, S. H.; Park, B. W.; Cheon, J. W. *J. Am. Chem. Soc.* **2011**, *133*, 7636.
(10) Tenne, R.; Margulis, L.; Genut, M.; Hodes, G. *Nature* **1992**, *360*, 444.
(11) Li, Y. F.; Zhou, Z.; Zhang, S. B.; Chen, Z. F. *J. Am. Chem. Soc.* **2008**, *130*, 16739.
(12) Kibsgaard, J.; Lauritsen, J. V.; Laegsgaard, E.; Clausen, B. S.; Topsoe, H.; Besenbacher, F. *J. Am. Chem. Soc.* **2006**, *128*, 13950.
(13) Wang, Z. Y.; Li, H.; Liu, Z.; Shi, Z.; Lu, J.; Suenaga, K.; Joung, S. K.; Okazaki, T.; Gu, Z. N.; Zhou, J.; Gao, Z. X.; Li, G. P.; Sanvito, S.; Wang, E.; Lijima, S. *J. Am. Chem. Soc.* **2010**, *132*, 13840.
(14) Seo, J. W.; Jun, Y. W.; Park, S. W.; Nah, H.; Moon, T.; Park, B.; Kim, J. G.; Kim, Y. J.; Cheon, J. *Angew. Chem., Int. Ed.* **2007**, *46*, 8828.
(15) Xiao, J.; Choi, D. W.; Cosimbescu, L.; Koech, P.; Liu, J.; Lemmon, J. P. *Chem. Mater.* **2010**, *22*, 4522.
(16) Wu, B.; Song, H.; Zhou, J.; Chen, X. *Chem. Commun.* **2011**, *47*, 8653.
(17) Golodnitsky, D.; Peled, E. *Electrochim. Acta* **1999**, *45*, 335.

(18) Xiao, J.; Wang, X. J.; Yang, X. Q.; Xun, S. D.; Liu, G.; Koech, P. K.; Liu, J.; Lemmon, J. P. *Adv. Funct. Mater.* **2011**, *21*, 2840.
(19) Feng, C. Q.; Ma, J.; Li, H.; Zeng, R.; Guo, Z. P.; Liu, H. K. *Mater. Res. Bull.* **2009**, *44*, 1811.
(20) Du, G.; Guo, Z. P.; Wang, S.; Zeng, R.; Chen, Z.; Liu, H. *Chem. Commun.* **2010**, *46*, 1106.
(21) Chang, K.; Chen, W. X. *J. Mater. Chem.* **2011**, *21*, 17175.
(22) Chang, K.; Chen, W. X. *ACS Nano* **2011**, *5*, 4720.
(23) Luo, B.; Fang, Y.; Wang, B.; Zhou, J. H.; Song, H. H.; Zhi, L. J. *Energy Environ. Sci.* **2012**, *5*, 5226.
(24) Chang, K.; Chen, W. X. *Chem. Commun.* **2011**, *47*, 4252.
(25) Wang, D. H.; Choi, D. W.; Li, J.; Yang, Z. G.; Nie, Z. M.; Kou, R.; Hu, D. H.; Wang, C. M.; Saraf, L. V.; Zhang, J. G.; Aksay, I. A.; Liu, J. *ACS Nano* **2009**, *3*, 907.
(26) Li, N.; Liu, G.; Zhen, C.; Li, F.; Zhang, L. L.; Cheng, H. M. *Adv. Funct. Mater.* **2011**, *21*, 1717.
(27) Wu, Z. S.; Ren, W. C.; Wen, L.; Gao, L. B.; Zhao, J. P.; Chen, Z. P.; Zhou, G. M.; Li, F.; Cheng, H. M. *ACS Nano* **2010**, *4*, 3187.
(28) Li, B. J.; Cao, H. Q.; Shao, J.; Li, G. Q.; Qu, M. Z.; Yin, G. *Inorg. Chem.* **2011**, *50*, 1628.
(29) Zhou, G. M.; Wang, D. W.; Li, F.; Zhang, L. L.; Li, N.; Wu, Z. S.; Wen, L.; Lu, G. Q.; Cheng, H. M. *Chem. Mater.* **2010**, *22*, 5306.
(30) Yoo, E. J.; Kim, J.; Hosono, E. J.; Zhou, H. S.; Kudo, T.; Honma, I. *Nano Lett.* **2008**, *8*, 2277.
(31) Zhang, F.; Cao, H. Q.; Yue, D. M.; Zhang, J. X.; Qu, M. Z. *Inorg. Chem.* **2012**, *51*, 9544.
(32) Hummers, W. S., Jr.; Offeman, R. E. *J. Am. Chem. Soc.* **1958**, *80*, 1339.
(33) Fan, X. B.; Peng, W. C.; Li, Y.; Li, X. Y.; Wang, S. L.; Zhang, G. L.; Zhang, F. B. *Adv. Mater.* **2008**, *20*, 4490.
(34) Li, Y. G.; Wang, H. L.; Xie, L. M.; Liang, Y. Y.; Hong, G. S.; Dai, H. J. *J. Am. Chem. Soc.* **2011**, *133*, 7296.
(35) Li, C. R.; Sun, Q. T.; Lu, N. P.; Chen, B. Y.; Dong, W. J. *J. Crystal. Growth* **2012**, *343*, 95.
(36) Yang, W. G.; Li, J. M.; Wang, Y. L.; Zhu, F.; Shi, W. M.; Wan, F. R.; Xu, D. S. *Chem. Commun.* **2011**, *47*, 1809.
(37) Ding, S. J.; Luan, D. Y.; Boey, F. Y. C.; Chen, J. S.; Lou, X. W. *Chem. Commun.* **2011**, *47*, 7155.
(38) Thomazeau, C.; Martin, V.; Afanasiev, P. *Appl. Catal., A* **2000**, *199*, 61.
(39) Manna, A. K.; Pati, S. K. *Chem.—Asian J.* **2009**, *4*, 855.
(40) Rao, A. M.; Eklund, P. C.; Bandow, S.; Thess, A.; Smalley, R. E. *Nature* **1997**, *388*, 257.
(41) Zhou, G. M.; Wang, D. W.; Yin, L. C.; Li, N.; Li, F.; Cheng, H. M. *ACS Nano* **2012**, *6*, 3214.
(42) Chen, J. M.; Wang, C. S. *Solid. State Commun.* **1974**, *14*, 857.
(43) Frey, G. L.; Tenne, R. *J. Mater. Res.* **1998**, *13*, 2412.
(44) Wang, H. W.; Skeldon, P.; Thompson, G. E. *Surf. Coat. Technol.* **1997**, *91*, 200.
(45) Liang, K. S.; Chianelli, R. R.; Chien, F. Z.; Moss, S. C. *J. Non-Cryst. Solids* **1986**, *79*, 251.
(46) Ding, S. J.; Zhang, D. Y.; Chen, J. S.; Lou, X. W. *Nanoscale* **2012**, *4*, 95.
(47) Ding, S. J.; Chen, J. S.; Lou, X. W. *Chem.—Eur J.* **2011**, *17*, 13142.
(48) Zou, Y. Q.; Wang, Y. *Nanoscale* **2011**, *3*, 2615.
(49) Chen, S. Q.; Wang, Y. *J. Mater. Chem.* **2010**, *20*, 9735.